Chinese Journal of
POLYMER SCIENCE

RESEARCH ARTICLE

https://doi.org/10.1007/s10118-023-3035-y
Chinese J. Polym. Sci. **2024**, *42*, 230–238

Impact of Annealing on the Melt Recrystallization of a-PDLA/*α*-PLLA Double-layered Films

Yun-Peng Li[a], Hao-Ran Shen[a], Shao-Juan Wang[a], Hao Zhang[a], Jian Hu[a], Rui Xin[a*], Xiao-Li Sun[b], and Shou-Ke Yan[a,b*]

[a] *Key Laboratory of Rubber-Plastics, Ministry of Education/Shandong Provincial Key Laboratory of Rubber-plastics, Qingdao University of Science & Technology, Qingdao 266042, China*
[b] *State Key Laboratory of Chemical Resource Engineering, Beijing University of Chemical Technology, Beijing 100029, China*

Electronic Supplementary Information

Abstract Poly(lactic acid) (PLA) as a bio-based polymer with biodegradability and biocompatibility has attracted much attention. To manipulate its properties for different applications, regulation of crystal structure and crystalline morphology becomes an attractive research topic. In this work, the structure evolution of layered samples containing an amorphous poly(D-lactide) (PDLA) layer and a crystalline poly(L-lactide) (PLLA) layer with highly oriented edge-on *α* lamellar crystals after annealing at 150 °C or/and after melt-recrystallization has been studied by AFM, FTIR, and TEM combined with electron diffraction. The results demonstrate that melt recrystallization of the as-prepared sample leads to the formation of abundant randomly oriented PLA stereo-complex (PLA SC) crystals. Annealing at 150 °C results in the formation of a small amount of oriented PLA SC crystals at the interface. These PLA SC crystals show great impact on the recrystallization behavior of sample after melting at 190 °C and then crystallizing at 90 °C. First, they impede the mutual diffusion of the overlying PDLA and underlying PLLA, and thus reduce their stereo-complexation ability as manifested by the decreased amount of PLA SC crystals. Second, they act as substrate to initiate the epitaxial crystallization of the overlying PDLA and underlying PLLA, which ensures the production of a highly oriented structure of PDLA and PLLA after melt recrystallization again.

Keywords Poly(L-lactide); Poly(D-lactide); Double layer; Stereocomplex

Citation: Li, Y. P.; Shen, H. R.; Wang, S. J.; Zhang, H.; Hu, J.; Xin, R.; Sun, X. L.; Yan, S. K. Impact of annealing on the melt recrystallization of a-PDLA/*α*-PLLA double-layered films. *Chinese J. Polym. Sci.* **2024**, *42*, 230–238.

INTRODUCTION

Poly(L-lactic acid) (PLLA) is a typical polymorphic polymer exhibiting at least four known crystal forms including the stable *α* form made of 10_3 helices arranged in an orthorhombic unit cell,[1–3] the *β* form made of 3_1 helices,[1,4] the *γ* form obtained through epitaxy,[5] and the *δ* (initially referred to as *α*′) grown at relative low temperature during melt or cold crystallization.[6,7] Besides, co-crystallization of it with its enantiomer, *i.e.*, poly(D-lactide) (PDLA), results in the formation of stereo-complex (SC) structure of the poly(lactide)s (PLAs), which exhibits some specific features, such as the outstanding heat resistance property with melting temperature about 50 ℃ higher than the PLLA and PDLA homogenous crystals (HCs), high nucleation efficiency toward the homo-crystallization of PLLA, and so on.[8–12]

It is well documented that the physical and mechanical properties of PLLA depend strongly on the polymorphism, crystallinity and crystalline morphology. For example, while the distinct PLLA crystal forms (*e.g.*, the *α* and *β* forms) exhibit different thermal stabilities, its tensile strength and modulus in the same *α* phase can be increased from 60 MPa and 3.7 GPa to 0.28–1 GPa and 7–10 GPa for randomly and highly oriented samples, respectively.[2,13] This makes the study on multiscale structure regulation of PLLA an attractive research topic, owing to the promising alternatives for commercial petrochemical-based polymers and potential applications in many fields.[14–19]

As is well-known, both previous thermal history of the materials and post annealing or thermal treatment provide efficient ways to regulate the crystal modification, crystallinity, and crystalline morphology of PLA.[20,21] To illustrate the impact of thermal history on the melt recrystallization behavior of PDLA/PLLA composite samples, double-layered films composited by a non-oriented amorphous PDLA (a-PDLA) layer and a highly oriented crystalline PLLA layer with edge-on *α* lamellar structure (*α*-PLLA) were fabricated. The structure evolution of them after annealing at 150 °C and melting at

* Corresponding authors, E-mail: xinrui0927@foxmail.com (R.X.)
E-mail: skyan@qust.edu.cn
skyan@mail.buct.edu.cn (S.K.Y.)

Received July 3, 2023; Accepted July 24, 2023; Published online September 15, 2023

190 °C then recrystallizing at 90° has been studied by means of atom force microscopy (AFM), Fourier transform infrared (FTIR) spectroscopy and transmission electron microscopy (TEM) combined with electron diffraction technique. It is found that a small amount of oriented PLA SC crystals with the same chain orientation as the used PLLA substrate film have formed at the interface layer after annealing at 150 °C. Meanwhile, epitaxy of PDLA on either oriented PLLA substrate or oriented PLA SC crystals takes place with the PDLA HCs oriented in the same way as the used PLLA substrate. Furthermore, the oriented SC crystals at the interface layer, even though in limited amount, show pronounced influence on the recrystallization behavior of the sample after melting at 190 °C.

EXPERIMENTAL

Materials

PLLA and PDLA materials used in this work were supplied by Changchun SinoBiomaterials Co., Ltd. The weight-average molecular weights of PLLA and PDLA are 2.2×10^5 g/mol and 9×10^4 g/mol, respectively. The optical purity of PDLA is 90%, while that of PLLA is 95%. Analytical *N*,*N*-dimethylformamide (DMF) and chloroform solvents were purchased from Beijing Chemical Reagent Co., Ltd.

Sample Preparation

Highly oriented PLLA ultrathin films with thickness ranging from 40 nm to 60 nm (as measured by Dektak XT step profiler, Bruker Corporation) were prepared according to a melt-draw technique,[22] which has frequently been used for getting highly oriented ultrathin films for different polymers, such as PLLA,[23,24] isotactic polybutene-1,[25,26] polyethylene,[27,28] isotactic polypropylene,[29–31] and poly(vinylidene fluoride).[32,33] In short, a small amount of 0.6 wt% PLLA solution in DMF was poured and spread uniformly on a preheated glass plate at 170 °C. After evaporation of the DMF solvent, the thin molten PLLA layer was then picked up by a motor-drive cylinder with a draw speed of 25 cm/s. An AFM phase image and a corresponding electron diffraction pattern of the as-prepared melt-drawn PLLA ultrathin films, which shows a peak melting temperature of 176 °C and an end melting temperature of 185 °C, are presented in Fig. S1 in the electronic supplementary information (ESI).[23] It is demonstrated that the as-prepared melt-drawn PLLA ultrathin films consist of granular crystallites (Fig. S1a in ESI). The corresponding electron diffraction (Fig. S1b in ESI) confirms the high orientation of the PLLA crystallites in *α* form with molecular chains or chain segments aligned along the melt-draw direction during sample preparation.

Amorphous PDLA films were prepared by spin-coating PDLA solution in chloroform with a concentration of 5 mg/mL on thin poly(acrylic acid) (PAA) substrate. The thickness of the as-prepared amorphous PDLA films is about 25 nm (measured by a Dektak XT step profiler, Bruker Corporation).

Double-layered samples composed of amorphous PDLA and oriented crystalline PLLA with *α* crystallites, hereafter denoted as a-PDLA/*α*-PLLA, were prepared by transferring the clean amorphous PDLA films, obtained through dissolving the PAA in PDLA/PAA composite films on the surface of distilled water, onto the surface of melt-drawn PLLA ultrathin films, which were supported by copper grid for TEM, silicon wafer for AFM, and KBr tablet for FTIR analyses. It should be mentioned here that while the annealing of a-PDLA/*α*-PLLA samples at 150 or 190 °C was performed by placing the sample directly on a hot-stage at desired temperatures, the cooling rate of samples from 190 °C to 90 °C was 50 °C/min.

Characterizations

A JEOL JEM-2100 TEM operated at 200 kV was used for TEM study. Exposure time for capturing the electron diffraction pattern is 3 s. AFM study was performed by a Bruker Dimension Icon AFM operated under tapping mode. The resonance frequency and spring constant of the tips used in this work are 75 kHz and 3 N/m, respectively. FTIR analysis was carried out on a Spectrum 100 FTIR spectrometer (PerkinElmer). Five a-PDLA/*α*-PLLA layers with the same PLLA orientation were used for enhancing the infrared signal. Polarized FTIR spectra were used to reveal the orientation of specimens. FTIR spectra were recorded in the wavenumber range from 4000 cm^{-1} to 450 cm^{-1} by averaging 32 scans at a 4 cm^{-1} resolution.

RESULTS

Morphology of a-PDLA/*α*-PLLA before and after Annealing at 150 °C

The morphologies of a-PDLA/*α*-PLLA samples before and after annealing at 150 °C for 5 h were first characterized by AFM. As presented in Figs. 1(a) and 1(b), the as-prepared sample, *i.e.*, a non-annealed a-PDLA/*α*-PLLA film, exhibits featureless and quite smooth surface due to the amorphous nature of the a-PDLA. After annealing at 150 °C for 5 h (Figs. 1c and 1d), isothermal cold crystallization of a-PDLA thin film on oriented *α*-PLLA film surface takes place, which results in the formation of parallel-aligned PDLA lamellar crystals arranged perpendicularly to the melt-draw direction of the *α*-PLLA as revealed by both the height (Fig. 1c) and phase (Fig. 1d) AFM images. This indicates the epitaxial crystallization of a-PDLA on oriented *α*-PLLA substrate with PDLA and PLLA molecular chains parallel to each other and has been further confirmed by the electron microscopy observation combined with electron diffraction.

Fig. 2 shows a bright field (BF) electron micrograph and an electron diffraction pattern of an annealed a-PDLA/*α*-PLLA sample as shown in Figs. 1(c) and 1(d). As can be seen from Fig. 2(a), the BF electron micrograph displays also a parallel-aligned lamellar structure, even though not as clear as the AFM images shown in Figs. 1(c) and 1(d). The appearance of sharp and well-defined reflection spots in the electron diffraction pattern shown in Fig. 2(b) confirms the high orientation of both PDLA and PLLA crystals. It should be noted that, except for the appearance of some new reflection spots, such as the (008) ones, the electron diffraction pattern shown in Fig. 2(b) is essentially the same as the one shown in Fig. S1(b) (in ESI). The appearance of some new diffraction spots is most probably due to the increased crystallinity caused by crystallization of PDLA and the perfection of *α*-PLLA crystals during annealing. Moreover, all of the reflection spots appeared in Fig. 2(b) can fully be indexed according to the *α* PLA crystalline unit cell with parameters a=10.683 Å, b=6.17 Å, c=28.86 Å.[34] This indicates unequivocally the occurrence of epitaxy of a-PDLA on oriented *α*-PLLA substrate also in *α* form. Moreover, the appearance of only one set diffraction spots

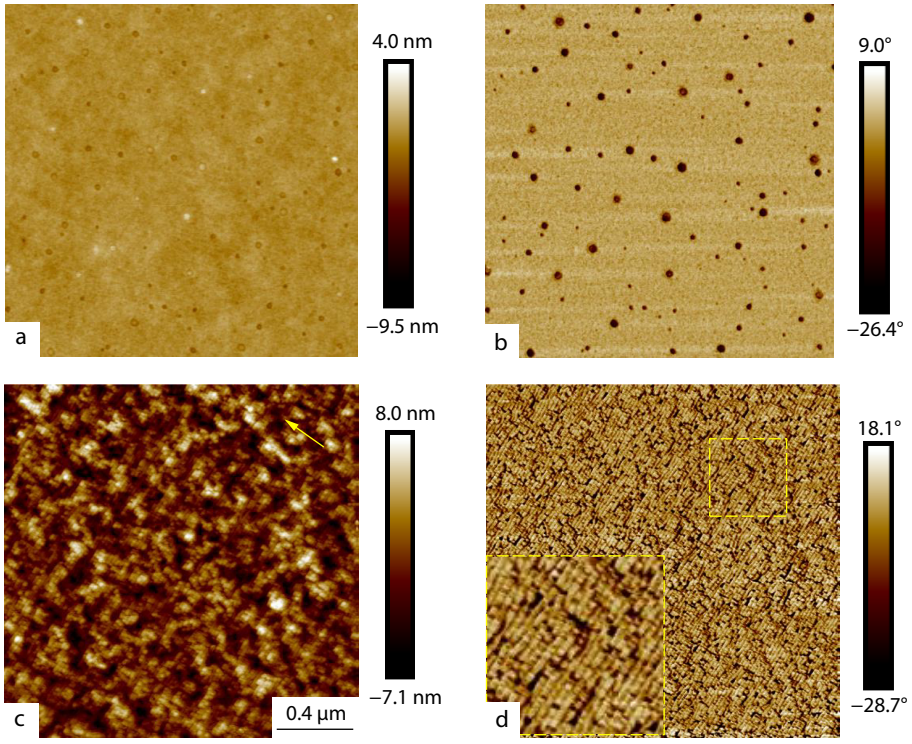

Fig. 1 AFM height (a, c) and phase (b, d) images of a-PDLA/*α*-PLLA samples before (a, b) and after (c, d) annealing at 150 °C for 5 h. The yellow arrow indicates the melt-draw direction of *α*-PLLA substrate film during preparation. The inset in (d) is the enlarged part marked by the yellow rectangle.

demonstrates the same orientation of both PLLA and PDLA crystals, indicating the same molecular chain alignments of them. This is comprehensive based on the exact same unit cell geometry and parameters of both PDLA and PLLA *α* form crystals, which creates a perfect matching between them with zero discrepancy. It has been reported that PLA SC crystals can form during annealing of the binary mixture of PLLA and PDLA single crystals at around 150 °C.[35] There are, however, no diffraction spots corresponding to the PLA SC crystals in Fig. 2(b).

Melt-recrystallization Behavior of Non-annealed and Annealed a-PDLA/*α*-PLLA Samples

The above experimental results demonstrate that epitaxial crystallization of amorphous PDLA layer in the a-PDLA/*α*-PLLA sample takes place on the oriented *α*-PLLA melt-drawn film during annealing at 150 °C. To show the effect of annealing on the melt recrystallization behavior of the a-PDLA/*α*-PLLA sample, melting of both a-PDLA and *α*-PLLA layers in the a-PDLA/*α*-PLLA sample at 190 °C for 5 min and then cooling the sample down to 90 °C at a rate of 50 °C/min for isothermal crystallization was performed. Figs. 3(a) and 3(b) present the AFM height and phase images of a non-annealed (*i.e.*, the as-prepared) a-PDLA/*α*-PLLA sample after melt recrystallization. Unlike the AFM images shown in Figs. 1(a) and 1(b), Figs. 3(a) and 3(b) show essentially a spherulitic morphology with edge-on lamellae. The lack of preferred orientation indicates the melting of oriented *α*-PLLA melt-drawn film, which has also been confirmed by the observation of non-oriented spherulitic

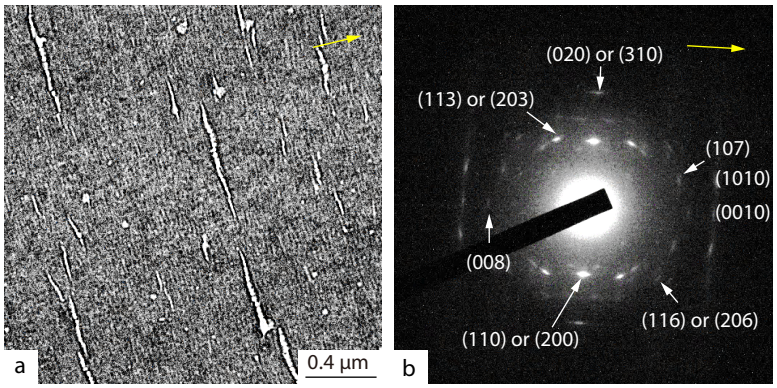

Fig. 2 A BF electron micrograph (a) and an electron diffraction pattern (b) of an annealed a-PDLA/*α*-PLLA sample as shown in Figs. 1(c) and 1(d). The yellow arrows indicate the molecular chain direction of the initially used *α*-PLLA melt-drawn films.

https://doi.org/10.1007/s10118-023-3035-y

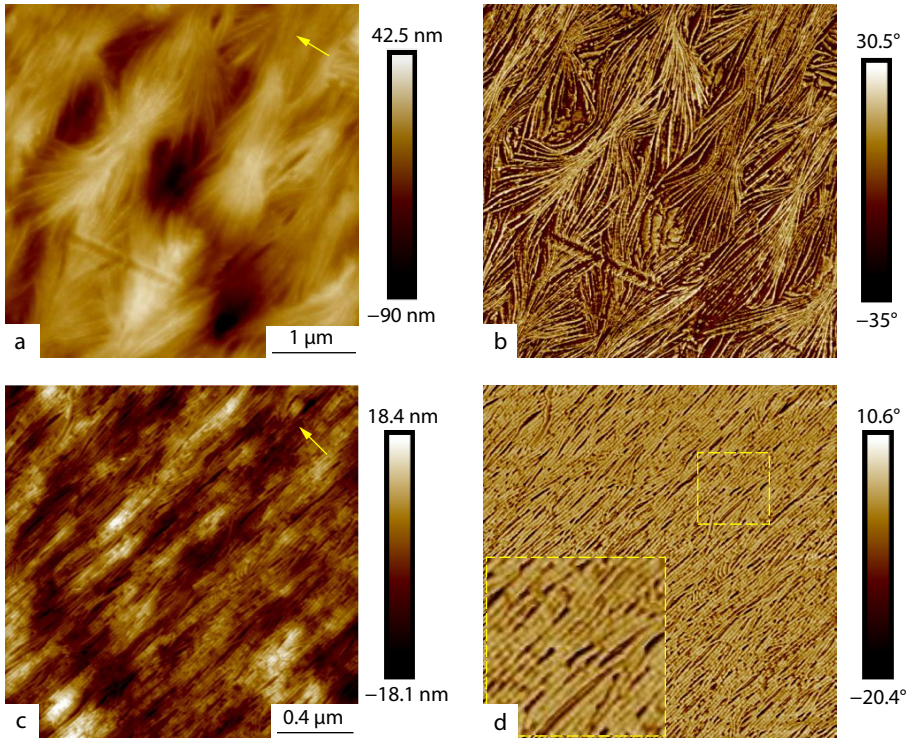

Fig. 3 AFM height (a, c) and phase (b, d) images of non-annealed (a, b) and annealed (c, d) a-PDLA/*α*-PLLA films after melting at 190 °C for 5 min and then recrystallizing isothermally at 90 °C for 5 h. The annealing of the sample shown in (c) and (d) was performed by placing the sample directly on a hot-stage at 150 °C for 5 h before melt-recrystallization. The yellow arrows indicate the molecular chain direction of the originally used *α*-PLLA. The inset in part (d) is the enlarged part marked by the yellow rectangle.

morphology of a single oriented *α*-PLLA layer after melting at 190 °C and then crystallizing at 90 °C for 5 h (*cf.* Fig. S2 in ESI), and thus both the molten underlying *α*-PLLA and overlying a-PDLA layers recrystallize in forms of spherulites. The morphology of the annealed a-PDLA/*α*-PLLA film after annealing at 190 °C for 5 min and then cooling down to 90 °C for 5 h is quite different from that of its non-annealed counterpart as revealed by AFM. As can be seen from Figs. 3(c) and 3(d), highly oriented lamellar structure with close resemblance to that shown in Figs. 1(c) and 1(d) appears again after melt recrystallization. The alignment of the oriented lamellae still perpendicular to the melt-draw direction of originally used *α*-PLLA substrate film indicates an oriented recrystallization of both PDLA and PLLA.

In order to further ascertain the different recrystallization behavior of non-annealed and annealed a-PDLA/*α*-PLLA films, TEM characterization of the samples after melt recrystallization has been performed. Fig. 4 shows the BF electron micrographs and corresponding electron diffraction patterns of the non-annealed and annealed a-PDLA/*α*-PLLA films after melting at 190 °C for 5 min and recrystallizing at 90 °C for 5 h. The BF micrograph of the non-annealed sample after melt recrystallization shown in Fig. 4(a) displays also the randomly oriented lamellar structure similar to the AFM images (*cf.* Figs. 3a and 3b). This is supported by the appearance of discontinued diffraction rings in the corresponding electron diffraction pattern shown in Fig. 4(b), which confirms melting of *α*-PLLA substrate film and a random orientation of both the PDLA and recrystallized PLLA crystals. On the other hand, the BF image of the annealed sample after melt recrystallization shown in Fig. 4(c) has a close resemblance with the one obtained before melt recrystallization presented in Fig. 2(a). The electron diffraction pattern related to the annealed sample after melt recrystallization shown in Fig. 4(d) with sharp and well defined reflection spots demonstrates the high orientation of the sample. It should be particularly noticed that, except for the reflection spots of *α*-PDLA and *α*-PLLA crystals observed originally in Fig. 2(b), some new diffractions corresponding to the (110), (211), (220) and (300) lattice planes of PLA SC crystals appear in Fig. 4(d). This implies the occurrence of stereo-complexation of PDLA and PLLA in the sample melt-recrystallized from the annealed a-PDLA/*α*-PLLA film, which has not been identified before melt recrystallization. The stereo-complexation happens actually also in the sample melt-recrystallized from the non-annealed a-PDLA/*α*-PLLA films as manifested by the appearance of (110), (220) and (300) reflection rings of the PLA SC crystals. The occurrence of stereo-complexation in melt-recrystallized samples has also been confirmed by the appearance of a high temperature melting peak at 221 °C.[36]

FTIR Analysis of the Samples Melt-recrystallized from Annealed and Non-Annealed a-PDLA/*α*-PLLA Double-layers

The electron diffraction results tell us unequivocally but qualitatively that melt recrystallization of a-PDLA/*α*-PLLA double-layers either before or after annealing at 150 °C promotes the stereo-complexation of PDLA and PLLA. To quantitatively characterize the amount of the PLA SC crystals,

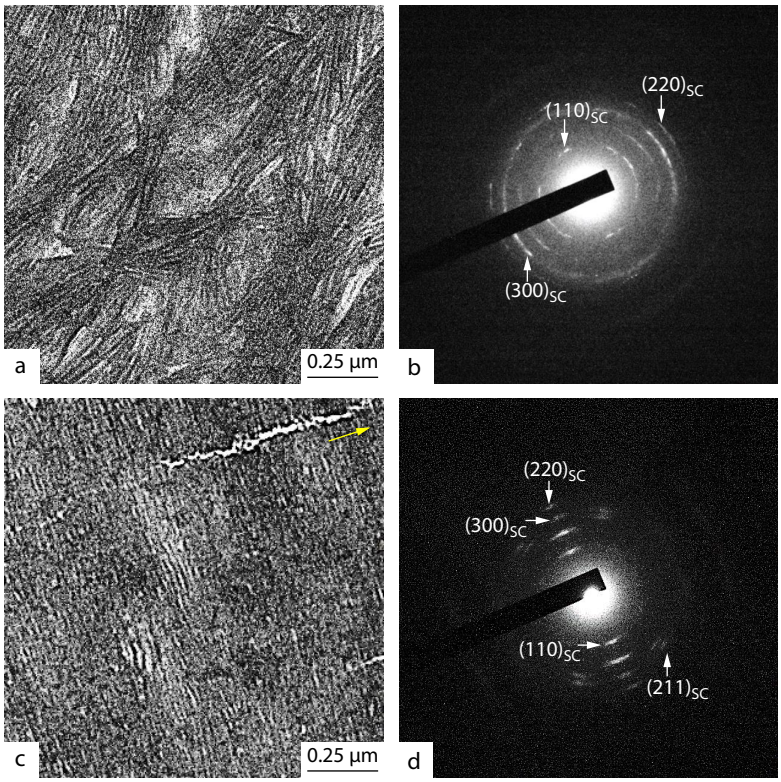

Fig. 4 BF micrographs (a, c) and corresponding electron diffraction patterns (b, d) of the samples melt-recrystallized from the non-annealed (a, b) and annealed (c, d) a-PDLA/*α*-PLLA double-layers at 90 °C for 5 h. The yellow arrow indicates the melt-draw direction of the used *α*-PLLA substrate film. In the electron diffraction patterns, only the reflection spots contributed by PDLA/PLLA stereo-complex crystals are indexed for clarity.

FTIR analyses of the samples melt-recrystallized from the non-annealed and annealed samples have been performed. Fig. 5 shows the FTIR spectra of the samples melt-recrystallized from non-annealed and annealed a-PDLA/*α*-PLLA films. From the top panels of Figs. 5(a) and 5(b), the characteristic band for the PLA SC crystals at 908 cm^{-1} can be clearly seen, indicating the occurrence of stereo-complexation in both samples. The band at 921 cm^{-1} typical for the *α*-PLA HCs appears only as a shoulder of the 908 cm^{-1} band.[37–39] This implies that the a-PDLA/*α*-PLLA films melt-recrystallize preferentially in form of PLA SC crystals. Generally, we can recognize that the amount of PLA SC crystals is higher in the sample recrystallized from non-annealed a-PDLA/*α*-PLLA films than in the sample recrystallized from annealed a-PDLA/*α*-PLLA films through comparing the relative intensity of 908 and 921 cm^{-1} bands. The quantitative calculation of the relative fraction of SC crystals (φ_{SC}) in a sample can be achieved by Eq. (1):

$$\varphi_{SC} = A_{908}/(A_{921} + A_{908}) \quad (1)$$

where A_{921} and A_{908} are the integral intensities of the related absorption bands. To this end, as presented in the bottom panels of Figs. 5(a) and 5(b), the FTIR spectra have been decomposed according to Gaussian functions for separating the overlapped 921 and 908 cm^{-1} absorption bands. The relative fractions of SC crystals in the samples melt-recrystallized from non-annealed and annealed a-PDLA/*α*-PLLA films are estimated to be 80.4% and 68.6%, respectively, manifesting the formation of SC crystals is easier in the non-annealed sample than in annealed sample.

DISCUSSION

According to the aforementioned experimental results, two issues should be discussed here. The first one is about the oriented melt recrystallization of the annealed sample. The used PLLA substrate films exhibit a peak melting temperature of *ca.* 176 °C and an end melting temperature of *ca.* 185 °C.[23] It will certainly be molten at 190 °C for 5 min. In this case, melt recrystallization of the non-annealed sample in randomly oriented structure can easily be understood. The oriented recrystallization of the annealed a-PDLA/*α*-PLLA films seems, however, hard to be understood. A possible reason may be the existence of some oriented PLA SC crystals at the interface of the annealed a-PDLA/*α*-PLLA sample, which can survive from melting at 190 °C and serve as oriented substrate to initiate the oriented recrystallization of both PDLA and PLLA. They have yet not been identified by the electron diffraction as presented in Fig. 2(b). This may be caused by the limited detecting sensitivity of electron diffraction. To check the validity of this hypothesis, FTIR study on five layers of the annealed samples has been conducted. As presented in Fig. 6(a), the 908 cm^{-1} band characteristic for the PLA SC crystals can indeed be recognized as a shoulder band of the 921 cm^{-1} band, which can be more clearly displayed in the decomposed spectra shown in Fig. 6(b). A fraction of 26% PLA SC crystals in the annealed sample

https://doi.org/10.1007/s10118-023-3035-y

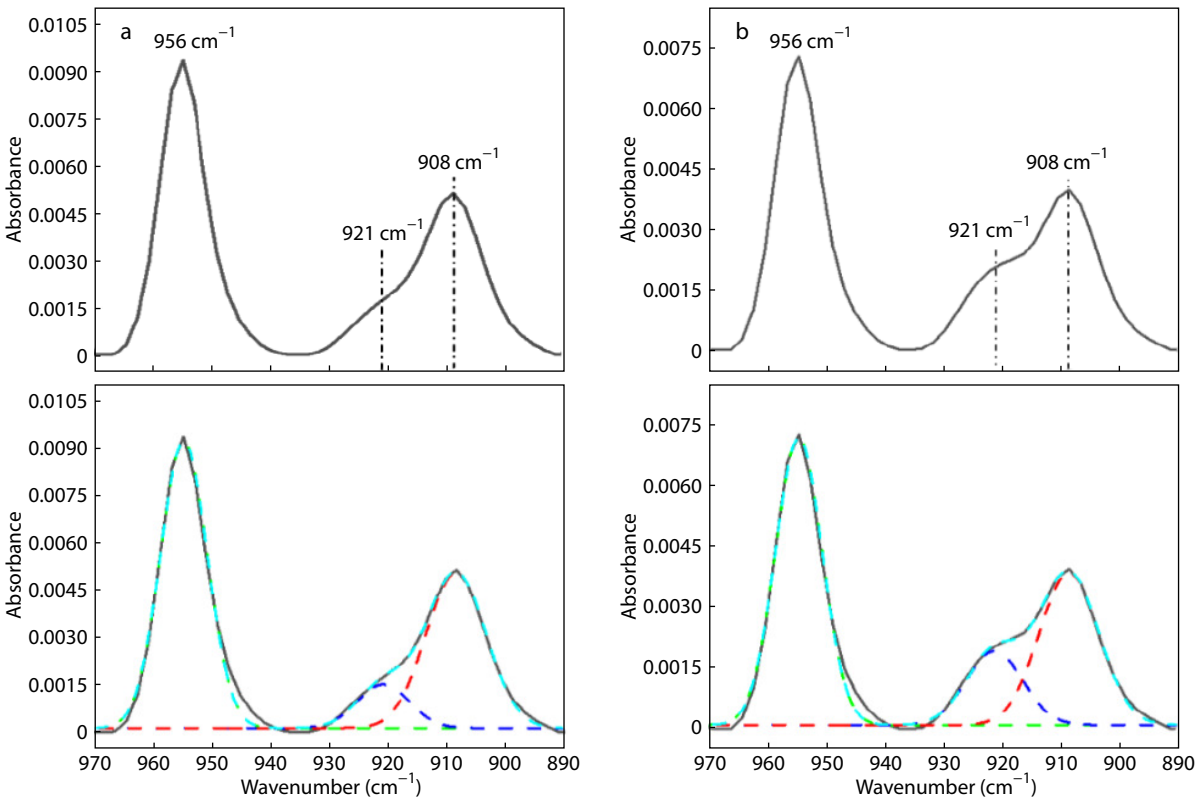

Fig. 5 Original (top panel) and corresponding decomposed (bottom panel) FTIR spectra of non-annealed (a) and annealed (b) a-PDLA/*α*-PLLA films after melting at 190 °C for 5 min and then isothermally crystallizing at 90 °C for 5 h.

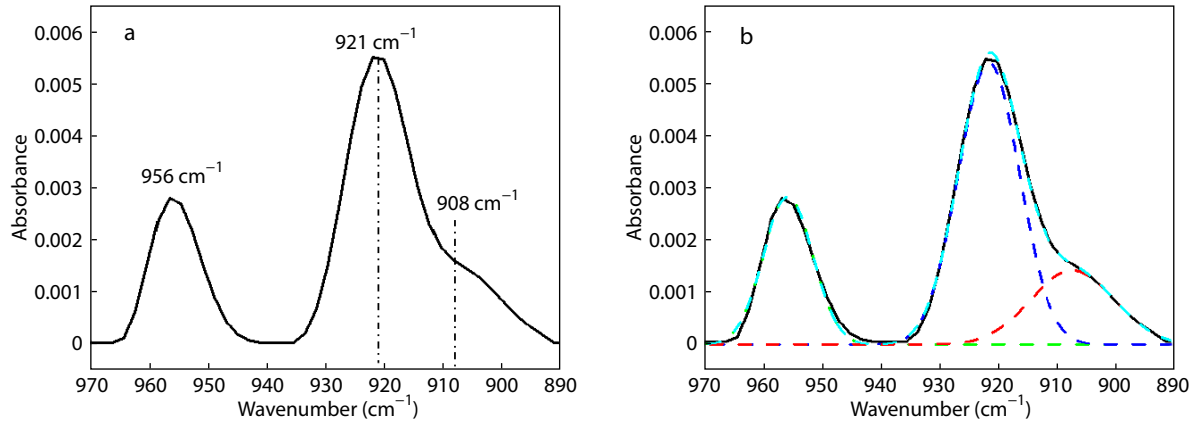

Fig. 6 Original (a) and corresponding decomposed (b) FTIR spectra of five a-PDLA/*α*-PLLA layers films after annealing at 150 °C for 5 h.

calculated according to Fig. 6(b) is obtained, which is really much smaller than that in the melt-recrystallized samples. These tiny PLA SC crystals should exist certainly at the interface between PDLA and PLLA. Moreover, the polarized FTIR spectra of the annealed a-PDLA/*α*-PLLA films measured with the electron vector perpendicular (90°) and parallel (0°) to the melt-draw direction of *α*-PLLA, see Fig. 7, do confirm the high orientation of both the PLA *α* HCs and SC crystals. This is reasonable since the as-prepared *α*-PLLA melt-drawn film exhibits excellent orientation and cannot be molten at 150 °C, which is far below the peak melting point of it.

From the above discussion, the oriented recrystallization of the annealed a-PDLA/*α*-PLLA film can be understood in the following way. As schematically illustrated in Fig. 8(a), the a-PDLA/*α*-PLLA film contains initially an amorphous PDLA layer and a crystalline PLLA layer with highly oriented edge-on lamellae in *α* form. Annealing this kind of sample at 150 °C produces a small amount of highly oriented PLA SC crystals at the interface between PDLA and *α*-PLLA layers as illustrated in Fig. 8(b), together with abundant highly oriented PDLA lamellae grown epitaxially either on ordered PLA SC crystals or PLLA lamellar crystals. When heating the sample up to 190 °C (Fig. 8c), the PLA SC crystals do not melt due to their high melting point at 221 °C rather than further grow at 190 °C laterally, while the PLA HCs melt. After cooling down to 90 °C (Fig. 8d), the highly oriented PLA SC crystals induce the

https://doi.org/10.1007/s10118-023-3035-y

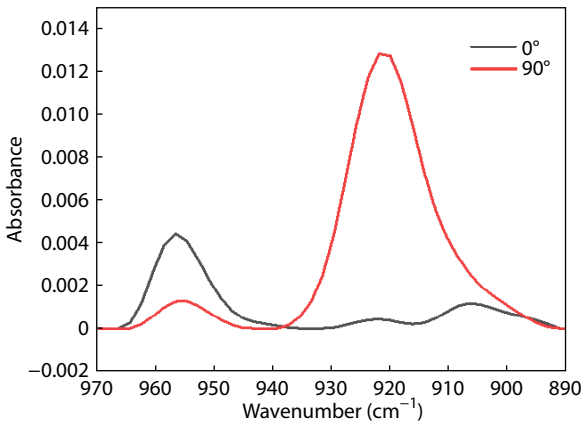

Fig. 7 Polarized FTIR spectra of five a-PDLA/*α*-PLLA layers with identical PLLA orientation after annealing at 150 °C for 5 h and measured with the electron vector perpendicular (90°) and parallel (0°) to the melt-draw direction of *α*-PLLA.

homo-crystallization of underlying molten PLLA and overlying molten PDLA through epitaxy, which has been confirmed to accelerate the crystallization rate tremendously,[40] and thus leads to the formation of a highly oriented lamellar structure again.

The second issue should be addressed is about the higher SC fraction in non-annealed sample than in annealed sample after melting at 190 °C and recrystallizing at 90 °C. This seems also difficult to be understood since parallel chain alignment of the PLLA and PDLA is expected to be favor of the formation of PLA SC crystals.[41] It can be actually explained in the following way. It is well known that the PLA SC crystals consist of PLLA and PDLA racemic helical pairs.[42] Taking this into account, the melting of both PDLA and PLLA films in the non-annealed a-PDLA/*α*-PLLA sample at 190 °C facilities the intermixing of PDLA and PLLA, which promotes the generation of PDLA and PLLA racemic helical pairs and thus favors the formation of PLA SC crystals. As a result, more PLA SC crystals, even though non-oriented, form after melt recrystallization. For the annealed a-PDLA/*α*-PLLA film, the PLA SC crystals formed at the interface as illustrated in Fig. 8(b) cannot be molten at 190 °C and thus suppress the mutual diffusion of PDLA and PLLA chains in the melts overlying and underlying the SC crystals, respectively. Therefore, either the overlying PDLA melt or the underlying PLLA melt can only crystallize epitaxially at the surface of the preformed SC crystals. This resembles the phase-separated PDLA/PLLA glassy films that have been confirmed to suppress the stereo-complex crystallization due to the lack of the racemic helical pairs.[38] In this case, although the PLA SC crystals formed at 150 °C can still grow transversely at the interface (Fig. 8c) and stereo-complex crystallization at places without preformed PLA SC crystals can take place in the same way as the non-annealed sample, the overall amount of SC crystals in the sample melt-recrystallized from the annealed a-PDLA/*α*-PLLA film will certainly be reduced. However, the epitaxial growth of both PDLA and PLLA HCs induced by oriented PLA SC crystals results in an oriented recrystallization of them.

CONCLUSIONS

In summary, structure evolution of a-PDLA/*α*-PLLA films containing an amorphous PDLA layer and a highly oriented PLLA layer with edge-on *α* crystalline lamellae after annealing at 150 °C or/and melt-recrystallizing isothermally at 90 °C has been studied by AFM, TEM and FTIR techniques. AFM and TEM results demonstrate that the amorphous PDLA can crystallize from the glassy state epitaxially on the oriented *α*-PLLA surface at 150 °C, leading to the formation of oriented edge-on lamellar structure with mainly *α* HCs. On the other hand, FTIR result obtained from five layers of annealed a-PDLA/*α*-PLLA sample reveals the formation of about 26.5% highly oriented PLA SC crystals during annealing at 150 °C.

Melting the as-prepared a-PDLA/*α*-PLLA film at 190 °C and then cooling down to 90 °C result in the recrystallization of both PDLA and PLLA, and the formation of abundant PLA SC crystals (*ca*. 80.4%) together with less than 20% PLA HCs. Both the PLA HCs and SC crystals are randomly oriented. The melt recrystallization of the a-PDLA/*α*-PLLA film annealed prior at 150 °C for 5 h leads, however, to the formation of highly oriented structure of both the PLA SC crystals and the PDLA and

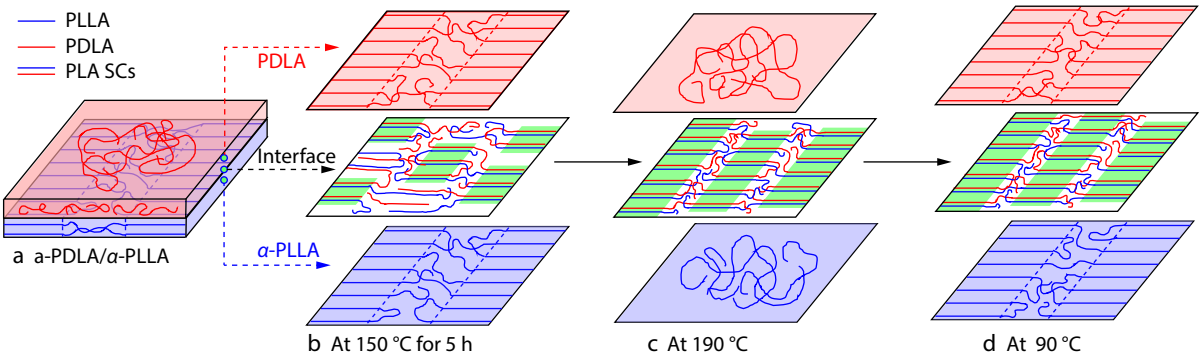

Fig. 8 Sketch illustrating the formation of highly oriented PLA SC crystals by annealing an a-PDLA/*α*-PLLA sample (a) at 150 °C for 5h (b) at the interface between PDLA and PLLA as indicated by the green color. These PLA SC crystals survive from melting and further grow at 190 °C laterally (c). By cooling the sample down to 90 °C for isothermal crystallization (d), the PDLA melt overlying the PLA SC crystals as well as the PLLA melt underlying the PLA SC crystals grow epitaxially at the PLA SC crystal surfaces, resulting in an oriented recrystallization of them.

https://doi.org/10.1007/s10118-023-3035-y

PLLA HCs. The oriented recrystallization of the annealed a-PDLA/α-PLLA film after melting at 190 °C has been associated to the small amount oriented PLA SC crystals existing at the interface. They grow further at 190 °C laterally and prevent mutual diffusion of the overlying PDLA and underlying PLLA, resulting in a relatively lower fraction of PLA SC crystals (68.6%) in the annealed a-PDLA/α-PLLA film after melt recrystallization compared to that in the non-annealed sample. On other hand, they serve as substrate and initiate the epitaxial crystallization of PDLA and PLLA after cooling down to 90 °C, ensuring an oriented recrystallization of them.

Conflict of Interests

Shou-Ke Yan is an associate editor for *Chinese Journal of Polymer Science* and was not involved in the editorial review or the decision to publish this article. All authors declare that there are no competing interests.

Electronic Supplementary Information

Electronic supplementary information (ESI) is available free of charge in the online version of this article at http://doi.org/10.1007/s10118-023-3035-y.

ACKNOWLEDGMENTS

This work was financially supported by the National Natural Science Foundation of China (Nos. 52027804 and 22022501), Postgraduate Independent Innovation Project (No. B2022KY004, Qingdao University of Science and Technology).

REFERENCES

1 Eling, B.; Gogolewski, S.; Pennings, A. J. Biodegradable materials of poly(L-lactic acid): 1. Melt-spun and solution-spun fibres. *Polymer* **1982**, *23*, 1587–1593.
2 De Santis, P.; Kovacs, A. J. Molecular conformation of poly(S-lactic acid). *Biopolymers* **1968**, *6*, 299–306.
3 Miyata, T.; Masuko, T. Morphology of poly(L-lactide) solution-grown crystals. *Polymer* **1997**, *38*, 4003–4009.
4 Hoogsteen, W.; Postema, A. R.; Pennings, A. J.; ten Brinke, G.; Zugenmaier, P. Crystal structure, conformation and morphology of solution-spun poly(L-lactide) fibers. *Macromolecules* **1990**, *23*, 634–642.
5 Cartier, L.; Okihara, T.; Ikada, Y.; Tsuji, H.; Puiggali, J.; Lotz, B. Epitaxial crystallization and crystalline polymorphism of polylactides. *Polymer* **2000**, *41*, 8909–8919.
6 Zhang, J.; Duan, Y.; Sato, H.; Tsuji, H.; Noda, I.; Yan, S.; Ozaki, Y. Crystal modifications and thermal behavior of poly(L-lactic acid) revealed by infrared spectroscopy. *Macromolecules* **2005**, *38*, 8012–8021.
7 Wasanasuk, K.; Tashiro, K. Crystal structure and disorder in poly(L-lactic acid) δ form (α′ form) and the phase transition mechanism to the ordered α form. *Polymer* **2011**, *52*, 6097–6109.
8 Ikada, Y.; Jamshidi, K.; Tsuji, H.; Hyon, S. H. Stereocomplex formation between enantiomeric poly(lactides). *Macromolecules* **1987**, *20*, 904–906.
9 Ju, Y. L.; Li, X. L.; Diao, X. Y.; Bai, H. W.; Zhang, Q.; Fu, Q. Mixing of racemic poly(L-lactide)/poly(D-lactide) blend with miscible poly(D,L-lactide): toward all stereocomplex-type polylactide with strikingly enhanced SC crystallizability. *Chinese J. Polym. Sci.* **2021**, *39*, 1470–1480.
10 Zheng, Y.; Pan, P. Crystallization of biodegradable and biobased polyesters: Polymorphism, cocrystallization, and structure-property relationship. *Prog. Polym. Sci.* **2020**, *109*, 101291.
11 Tsuji, H.; Fukui, I. Enhanced thermal stability of poly(lactide)s in the melt by enantiomeric polymer blending. *Polymer* **2003**, *44*, 2891–2896.
12 Schmidt, S. C.; Hillmyer, M. A. Polylactide stereocomplex crystallites as nucleating agents for isotactic polylactide. *J. Polym. Sci., Part B: Polym. Phys.* **2001**, *39*, 300–313.
13 Perego, G.; Cella, G. D.; Bastloll, C. Effect of molecular weight and crystallinity on poly(lactic acid) mechanical properties. *J. Appl. Polym. Sci.* **1996**, *59*, 37–43.
14 Garlotta, D. A literature review of poly(lactic acid). *J. Polym. Environ.* **2001**, *9*, 63–84.
15 Nair, L. S.; Laurencin, C. T. Biodegradable polymers as biomaterials. *Prog. Polym. Sci.* **2007**, *32*, 762–798.
16 Gupta, B.; Revagade, N.; Hilborn, J. Poly(lactic acid) fiber: an overview. *Prog. Polym. Sci.* **2007**, *32*, 455–482.
17 Ma, X. B.; Yang, R.; Sekhar, K. P. C.; Chi, B. Injectable hyaluronic acid/poly(γ-glutamic acid) hydrogel with step-by-step tunable properties for soft tissue engineering. *Chinese J. Polym. Sci.* **2021**, *39*, 957–965.
18 Tsuji, H. Poly(lactic acid) stereocomplexes: a decade of progress. *Adv. Drug Deliv. Rev.* **2016**, *107*, 97–135.
19 Xu, Y.; Yang, J.; Liu, Z. F.; Zhou, Z. P.; Liang, Z. P.; Hao, T. F.; Nie, Y. J. Stereocomplex crystallization in asymmetric diblock copolymers studied by dynamic monte carlo simulations. *Chinese J. Polym. Sci.* **2021**, *39*, 632–639.
20 Zhang, Z. C.; Gao, X. R.; Hu, Z. J.; Yan, Z.; Xu, J. Z.; Xu, L.; Zhong, G. J.; Li, Z. M. Inducing stereocomplex crystals by template effect of residual stereocomplex crystals during thermal annealing of injection-molded polylactide. *Ind. Eng. Chem. Res.* **2016**, *55*, 10896–10905.
21 Huang, Y. F.; Zhang, Z. C.; Li, Y.; Xu, J. Z.; Xu, L.; Yan, Z.; Zhong, G. J.; Li, Z. M. The role of melt memory and template effect in complete stereocomplex crystallization and phase morphology of polylactides. *Cryst. Growth Des.* **2018**, *18*, 1613–1621.
22 Petermann, J.; Gohil, R. M. A new method for the preparation of high modulus thermoplastic films. *J. Mater. Sci.* **1979**, *14*, 2260–2264.
23 Li, Y.; Xin, R.; Wang, S.; Guo, Z.; Sun, X.; Ren, Z.; Li, H.; Li, L.; Yan, S. Structure and mechanical property of melt-drawn oriented PLA ultrathin films. *Macromolecules* **2021**, *54*, 9124–9134.
24 Li, Y.; Wang, S.; Zhang, H.; Hu, J.; Liu, Q.; Xin, R.; Yan, S. Structure evolution of oriented poly(L-lactic acid) ultrathin films during deformation. *Macromolecules* **2022**, *55*, 6633–6643.
25 Li, Y.; Guo, Z.; Xue, M.; Yan, S. Epitaxial recrystallization of *i*PBu in form II on oriented *i*PS film initially induced by oriented form I *i*PBu. *Macromolecules* **2019**, *52*, 4232–4239.
26 Yan, S. Origin of oriented recrystallization of carbon coated pre-oriented ultra-thin polymer films. *Macromolecules* **2003**, *36*, 339–345.
27 Li, H.; Liu, D.; Bu, X.; Zhou, Z.; Ren, Z.; Sun, X.; Reiter, R.; Yan, S.; Reiter, G. Formation of asymmetric leaf-shaped crystals in ultrathin films of oriented polyethylene molecules resulting from high-temperature relaxation and recrystallization. *Macromolecules* **2020**, *53*, 346–354.

28 Zhou, H.; Jiang, S.; Yan, S. Epitaxial crystallization of poly(3-hexylthiophene) on a highly oriented polyethylene thin film from solution. *J. Phys. Chem. B* **2011**, *115*, 13449–13454.
29 Ma, L.; Zhou, Z.; Zhang, J.; Sun, X.; Li, H.; Zhang, J.; Yan, S. Temperature-dependent recrystallization morphologies of carbon-coated isotactic polypropylene highly oriented thin films. *Macromolecules* **2017**, *50*, 3582–3589.
30 Guo, Z.; Yuan, C.; Song, C.; Xin, R.; Hou, C.; Hu, J.; Li, H.; Sun, X.; Ren, Z.; Yan, S. Temperature-dependent reversibility of epitaxy between isotactic polystyrene and polypropylene. *Macromolecules* **2021**, *54*, 7564–7571.
31 Guo, Z.; Xin, R.; Hu, J.; Li, Y.; Sun, X.; Yan, S. Direct high-temperature form I crystallization of isotactic poly(1-butene) assisted by oriented isotactic polypropylene. *Macromolecules* **2019**, *52*, 9657–9664.
32 Liu, J.; Zhao, Q.; Dong, Y.; Sun, X.; Hu, Z.; Dong, H.; Hu, W.; Yan, S. Self-polarized poly(vinylidene-fluoride) ultrathin film and its piezo/ferroelectric properties. *ACS Appl. Mater. Interfaces* **2020**, *12*, 29818–29825.
33 Dong, Y.; Wu, J.; Hu, J.; Yan, S.; Müller, A. J.; Sun, X. Thermal-field-tuned heterogeneous amorphous states of poly(vinylidene fluoride) films with precise transition from nonpolar to polar phase. *Macromolecules* **2022**, *55*, 9671–9679.
34 Wasanasuk, K.; Tashiro, K.; Hanesaka, M.; Ohhara, T.; Kurihara, K.; Kuroki, R.; Tamada, T.; Ozeki, T.; Kanamoto, T. Crystal structure analysis of poly(L-lactic acid) α form on the basis of the 2-dimensional wide-angle synchrotron X-ray and neutron diffraction measurements. *Macromolecules* **2011**, *44*, 6441–6452.
35 Fujita, M.; Sawayanagi, T.; Abe, H.; Tanaka, T.; Iwata, T.; Ito, K.; Fujisawa, T.; Maeda, M. Stereocomplex formation through reorganization of poly(l-lactic acid) and poly(D-lactic acid) crystals. *Macromolecules* **2008**, *41*, 2852–2858.
36 Li, Y.; Shen, H.; Wang, S.; Zhang, H.; Hu, J.; Xin, R.; Yan, S. Structure evolution of amorphous poly(D-lactic acid) on highly oriented poly(L-lactic acid) film during annealing. *Polymer* **2023**, *280*, 126037.
37 Zhang, J.; Tashiro, K.; Tsuji, H.; Domb, A. J. Investigation of phase transitional behavior of poly(L-lactide)/poly(D-lactide) blend used to prepare the highly-oriented stereocomplex. *Macromolecules* **2007**, *40*, 1049–1054.
38 Liu, J.; Qi, X.; Feng, Q.; Lan, Q. Suppression of phase separation for exclusive stereocomplex crystallization of a high-molecular-weight racemic poly(L-lactide)/poly(D-lactide) blend from the glassy state. *Macromolecules* **2020**, *53*, 3493–3503.
39 Yan, J.; Zheng, Y.; Zhou, Y.; Liu, Y.; Tan, H.; Fu, Q.; Ding, M. Application of infrared spectroscopy in the multiscale structure characterization of poly(L-lactic acid). *Polymer* **2023**, *278*, 125985.
40 Zhang, H.; Song, Y.; Li, N.; Wang, S.; Hu, J.; Xin, R.; Zhang, J.; Song, C.; Yan, S. Influence of freezing layer on the crystallization kinetics of PCL on oriented PE film. *Chinese J. Polym. Sci.* **2023**, *41*, 778–786.
41 Xiong, Z.; Liu, G.; Zhang, X.; Wen, T.; de Vos, S.; Joziasse, C.; Wang, D. Temperature dependence of crystalline transition of highly-oriented poly(L-lactide)/poly(D-lactide) blend: *in-situ* synchrotron X-ray scattering study. *Polymer* **2013**, *54*, 964–971.
42 Yang, C. F.; Huang, Y. F.; Ruan, J.; Su, A. C. Extensive development of precursory helical pairs prior to formation of stereocomplex crystals in racemic polylactide melt mixture. *Macromolecules* **2012**, *45*, 872–878.

https://doi.org/10.1007/s10118-023-3035-y